ELSEVIER

Earth and Planetary Science Letters 204 (2002) 115–132

EPSL

www.elsevier.com/locate/epsl

Three-dimensional passive flow and temperature structure beneath oceanic ridge–ridge–ridge triple junctions

Jennifer E. Georgen [a,*], Jian Lin [b]

[a] *MIT–WHOI Joint Program in Oceanography, Woods Hole Oceanographic Institution, Woods Hole, MA 02543, USA*
[b] *Department of Geology and Geophysics, Woods Hole Oceanographic Institution, Woods Hole, MA 02543, USA*

Received 12 March 2002; received in revised form 4 September 2002; accepted 6 September 2002

Abstract

This study uses numerical modeling to investigate generalized characteristics of mantle flow and thermal structure in the vicinity of ridge–ridge–ridge (RRR) triple junctions. Oceanic triple junctions present a unique opportunity to study three-dimensional (3D) mantle dynamics in a tectonic setting considerably different than where only two plates diverge. In many prominent oceanic triple junctions, including Rodrigues, Azores, and Galapagos, the slowest-spreading ridge branch intersects the near-collinear faster-spreading branches quasi-orthogonally. This study focuses on triple junctions free of influence from nearby hotspots, similar to the geometry of the Rodrigues Triple Junction. A finite element model was used to calculate the steady-state 3D velocity flow field and temperature patterns resulting from advective and conductive heat transfer. For the slowest-spreading branch, model results predict a strong component of along-axis velocity directed away from the triple junction. Both upwelling velocity and temperature are calculated to increase along the slowest-spreading ridge toward the triple junction, approaching the upwelling rate and temperature of the fastest-spreading branch. Within 200 km of the triple junction, upwelling velocity is predicted to increase more than threefold along the slowest-spreading ridge. In contrast, the calculated upwelling velocity and temperature for the fastest-spreading branch are not significantly different from the case of a single spreading ridge. For triple junctions where the three ridges spread faster than the Rodrigues Triple Junction system, such as the Galapagos Triple Junction, the contrast in axial upwelling velocity and temperature between the slowest- and fastest-spreading ridges is predicted to be less significant. However, for triple junctions with overall slower spreading velocities, such as the Azores Triple Junction, this contrast is more pronounced.

Keywords: Rodrigues Triple Junction; Southwest Indian Ridge; triple junctions; mid-ocean ridges; mantle dynamics

1. Introduction

Triple junctions, defined as the location where three plate boundaries meet, mark an important geological setting along the global mid-ocean ridge system. Triple junctions are geometrically required features of a planet with more than two tectonic plates. Because of their unusual con-

* Corresponding author. Present address: Graduate School of Oceanography, University of Rhode Island, 232 Horn Laboratory, South Ferry Road, Narragansett, RI 02882, USA. Tel.: +1-401-874-6684; Fax: +1-401-874-6811.
E-mail addresses: jgeorgen@gsosun1.gso.uri.edu (J.E. Georgen), jlin@whoi.edu (J. Lin).

0012-821X/02/$ – see front matter © 2002 Elsevier Science B.V. All rights reserved.
PII: S0012-821X(02)00953-6

figuration, triple junctions provide a unique tectonic window for studying mantle and lithospheric dynamics. For example, at an oceanic ridge–ridge–ridge (RRR) triple junction, the upwelling patterns of three spreading centers interact, revealing information about mantle dynamics beyond what can be learned from the case of a single ridge.

Several studies have addressed the plate kinematics, geophysics, and seafloor morphology of triple junctions. For example, using constraints from GLORIA sidescan sonar data, Mitchell and Parson [1] investigated the long-term evolution of ridge segmentation at the Rodrigues Triple Junction (RTJ, Fig. 1a) in the central Indian Ocean. Searle [2] and Searle and Francheteau [3] used bathymetric and GLORIA sidescan data to study the seafloor fabric and history of rift propagation at the Azores Triple Junction (ATJ, Fig. 1b) and the Galapagos Triple Junction (GTJ, Fig. 1c), respectively. Sclater et al. [4] interpreted magnetic data to show that the Bouvet Triple Junction (BTJ, Fig. 1d) in the southern Atlantic Ocean has alternated between RRR and ridge–fault–fault (RFF) configuration.

Numerical geodynamics models of 3D mantle flow for a single ridge system have greatly aided our understanding of ridge crustal and mantle geodynamics (e.g., [5–8]). However, no numerical models of 3D triple junction mantle flow have been developed to date. The purpose of this study is to explore long-wavelength patterns of mantle flow and temperature beneath oceanic RRR triple junctions. We first examine three oceanic RRR triple junctions, Rodrigues, Azores, and Galapagos, to synthesize their geometric commonalities and develop a generic triple junction configuration for use in modeling. We then use this generic geometry as the basis for 3D numerical calculations predicting mantle velocity and temperature structure for an RRR spreading system. We quantify how the triple junction configuration can induce along-axis flow and cause thermal perturbations, and we compare model predictions to observational data from the RTJ.

2. Triple junction geometry

Each branch of a triple junction may be a ridge, trench, or transform fault. Theoretically, 16 possible triple junction configurations exist, although not all are stable. The velocity vector method used to assess triple junction stability [9] shows that only the RRR configuration is stable for all spreading rates and boundary orientations. This investigation explores long-wavelength flow and thermal patterns around a generic RRR triple junction that captures the salient geometrical characteristics of the RTJ, and is very similar to the ATJ and GTJ. The kinematics of each of these three triple junctions is described below.

2.1. RRR triple junctions

The RTJ, also referred to as the Indian Ocean Triple Junction, is composed of the Southeast Indian Ridge (SEIR), Central Indian Ridge (CIR), and Southwest Indian Ridge (SWIR), with half-spreading rates of 2.9, 2.4, and 0.7 cm/yr, respectively [10–11] (Fig. 1a). The SEIR and CIR are nearly collinear, and are intersected quasi-orthogonally by the SWIR [10]. The RTJ has been stable for at least the last 5–10 Myr, and perhaps for as long as 40 Myr [10,12]. For the last ~80 Myr, the RTJ has been propagating eastward [13]; since 10 Ma, the SWIR and CIR have lengthened by an average of 2.7 and 1.3 cm/yr, respectively [10].

→

Fig. 1. Location maps for four RRR triple junctions: (a) Rodrigues, (b) Azores, (c) Galapagos, and (d) Bouvet. Ridge coordinates are from [56], and free-air gravity data were extracted from the global satellite altimetry database of [57]. For each triple junction, the location of the 35 mGal contour is indicated, and an artificial illumination is applied from the NNW. The position of the nearest hotspot to each triple junction is shown with a star. Ridge abbreviations are as follows: SWIR = Southwest Indian Ridge, CIR = Central Indian Ridge, SEIR = Southeast Indian Ridge, N. MAR = Mid-Atlantic Ridge to the north of the Azores Triple Junction, S. MAR = Mid-Atlantic Ridge to the south of the Azores Triple Junction, Ter. R. = Terceira Rift, N. EPR = East Pacific Rise to the north of the Galapagos Triple Junction, S. EPR = East Pacific Rise to the south of the Galapagos Triple Junction, GSC = Galapagos Spreading Center, and AAR = American Antarctic Ridge.

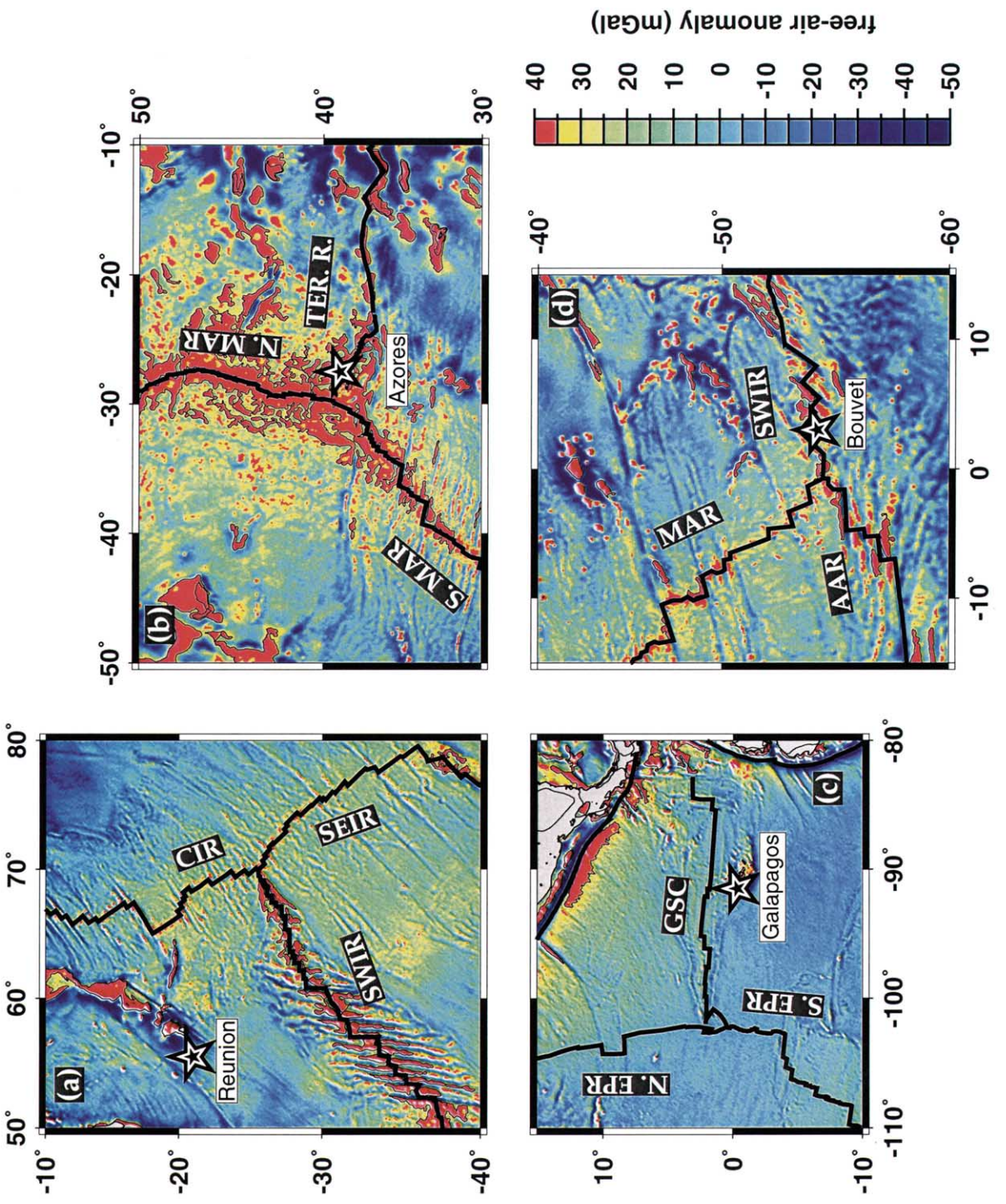
free-air anomaly (mGal)
40
30
20
10
0
-10
-20
-30
-40
-50
(a)
Reunion
CIR
SEIR
SWIR
(b)
Azores
TER. R.
N. MAR
S. MAR
(c)
Galapagos
GSC
S. EPR
N. EPR
(d)
Bouvet
SWIR
MAR
AAR

The nearest hotspot, Reunion, is at present more than 1000 km from the RTJ, and therefore is presumed not to directly affect the mantle geodynamics of the RTJ.

The GTJ marks the intersection of a northern branch of the East Pacific Rise (N. EPR), a southern branch of the East Pacific Rise (S. EPR), and the Galapagos Spreading Center (GSC) (Fig. 1c). The GSC opens at a rate of 2.1 cm/yr, while half-rates for the N. EPR and S. EPR are 6.9 cm/yr and 6.8 cm/yr, respectively [14]. Locally, the Galapagos Microplate complicates the tectonics of the GTJ. The Galapagos Microplate has an area of 13 000 km^2 and rotates clockwise at 6°/Myr [15]. Although the Galapagos plume imparts significant bathymetric, seismic, gravity, and geochemical anomalies to the GSC [16–20], it is located more than 1000 km away from the GTJ, making it unlikely that it directly influences GTJ geodynamics.

In contrast to the RTJ and GTJ, both the ATJ and the BTJ are affected by the presence of a nearby hotspot. The ATJ (Fig. 1b) is composed of a northern branch of the Mid-Atlantic Ridge (N. MAR, half-rate 1.2 cm/yr), a southern branch of the Mid-Atlantic Ridge (S. MAR, half-rate 1.1 cm/yr), and the slow-opening Terceira Rift (Ter. R., half-rate 0.3 cm/yr). It has evolved from RFF to its present RRR configuration since its formation 45 Ma [2,21]. Searle [2] pointed out that de-

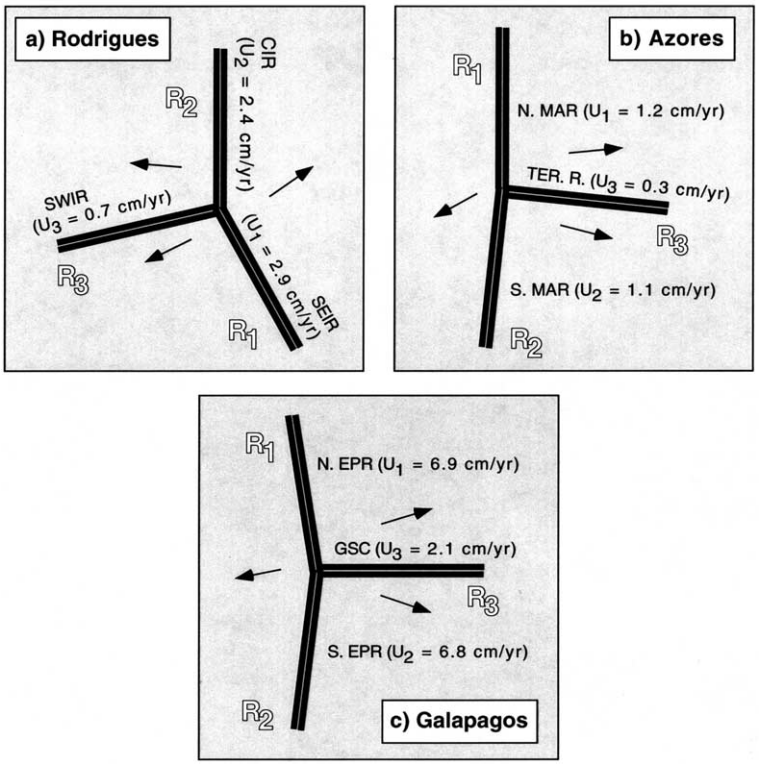

Fig. 2. Simplified geometry of the (a) RTJ, (b) ATJ, and (c) GTJ. Simplified geometry reflects the regional trend of each of the three spreading branches comprising a given triple junction, omitting transform offsets, microplates, and small zones of disconnectivity between the ridges and the virtual triple junction point. The half-spreading rate for each spreading branch is indicated, and ridge abbreviations are given in Fig. 1. Arrows show plate motion with respect to the triple junction, modified from [10] for (a), [2] for (b), and [3] for (c). R_1 designates the ridge with the fastest half-spreading rate U_1, R_2 the ridge with an intermediate-spreading rate U_2, and R_3 the ridge with the slowest-spreading rate U_3. In all three of the RTJ, ATJ, and GTJ, the two fastest-spreading ridges are nearly collinear, and are intersected quasi-perpendicularly by the slowest-spreading ridge. The ridge configuration is different, however, for the Bouvet Triple Junction (BTJ), where the three ridges have more equal separation angles from each other.

tailed understanding of the evolution of the ATJ is complicated by extremely slow spreading rates along the Ter. R. and the resultant lack of identifiable magnetic anomalies. The Azores hotspot significantly affects crustal accretion processes at the ATJ. Consistent with the general position of a broad S-wave seismic velocity anomaly [22], the distribution of recent volcanism in the Azores Archipelago suggest that the center of excess hotspot magma flux is approximately 100–200 km to the east of the MAR, at approximately the location of Faial Island [23]. The Azores hotspot imparts long-wavelength bathymetric, geochemical, and gravity gradients over a distance of ~1500–2000 km along the MAR, from the Kane FZ to approximately 44°N (e.g., [24–28]).

The SWIR, American Antarctic Ridge (AAR), and MAR join at the BTJ (Fig. 1d). These ridges have half-spreading rates of 0.8, 0.9, and 1.6 cm/yr, respectively [4], and are spaced at roughly equal angles from one another. Sclater et al. [4] suggested that over the past 20 Myr, the BTJ has spent 15 Myr in an RFF configuration and 5 Myr in the RRR mode, which is the current geometry. Ligi et al. [29] confirmed that the BTJ is locally RRR using high-resolution bathymetric, gravity, and magnetics data. The BTJ is associated with three hotspot-like melting anomalies within a 500-km radius, the Bouvet and Shona hotspots and Spiess Seamount [29–35]. However, the volcanic constructional features of all three anomalies are volumetrically small compared to islands such as Hawaii, Iceland, and Reunion (e.g., [36]).

Three of the four triple junctions described above have similar geometry. In each of the RTJ, ATJ, and GTJ, the two fastest-spreading ridges have nearly equal spreading rates and are roughly collinear, forming a trend which the slowest-spreading ridge intersects quasi-orthogonally (Fig. 2). This geometric similarity is shown quantitatively in Fig. 3, where U_1, U_2, and U_3 are the spreading rates of the fastest, intermediate, and slowest-spreading ridges, respectively. For all of the RTJ, ATJ, and GTJ, U_1/U_2 is 1.0–1.2, while U_1/U_3 is 3.3–4.1. In contrast, the BTJ has considerably different geometry as well as significantly different spreading velocity ratios. In this study,

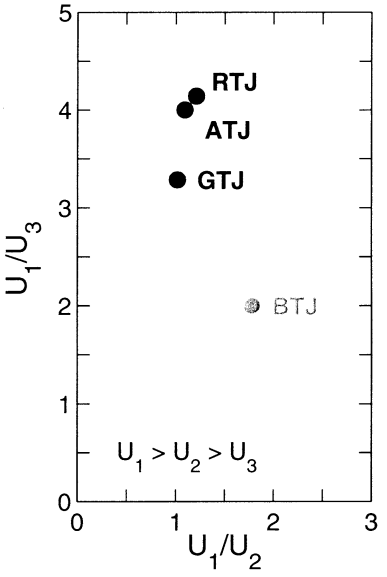

Fig. 3. The geometric similarity of the Rodrigues (RTJ), Azores (ATJ), and Galapagos (GTJ) triple junctions is shown in this plot of half-spreading rate ratios. For each triple junction, half-rates for the three ridges are U_1, U_2, and U_3, with $U_1 > U_2 > U_3$. Note that the RTJ, ATJ, and GTJ show similar spreading rate ratios, but ratios for the BTJ are significantly different.

we focus only on a generic RRR triple junction with geometric characteristics based on the RTJ, and similar to the ATJ and GTJ.

2.2. Simplified triple junction kinematics

The primary objective of this investigation is to examine how the long-wavelength mantle dynamics beneath a triple junction differ from that of a single ridge, and thus a simplified geometry is used to characterize triple junction plate kinematics. Rather than explicitly incorporating local, detailed ridge and transform segmentation patterns, we approximate the overall geometry of a given spreading center using a single, straight ridge aligned according to its regional, average strike. Diagrams of the simplified RTJ, ATJ, and GTJ are shown in Fig. 2. This simplification is desirable for illustrating the essential features of mantle upwelling patterns beneath a triple junction. This approximation, therefore, also ignores features such as microplates, as in the case of the

GTJ. Furthermore, for a number of triple junctions, including the RTJ [37], the three ridge branches fail to meet at a strict 'triple point', instead being joined by a zone of diffuse deformation near the 'virtual' triple junction. The gap distance between the termination of well-defined spreading along any given ridge axis and the virtual triple point is less than 100 km for all of the triple junctions considered here [2,29,38], again considerably shorter than the much longer wavelength patterns that are the subject of this investigation. The effects of these complexities are discussed qualitatively in a later section.

Because the RTJ is not affected by a nearby hotspot, we selected it as the basis for our numerical model. In the first model explored (Model 1), the half-spreading rates of the three ridge branches are set equal to the spreading rates of the SEIR, CIR, and SWIR. We denote the ridge with the relatively fastest-spreading rate U_1 as R_1. Similarly, the ridge with an intermediate-spreading rate is R_2, and the slowest-spreading ridge is R_3.

3. Numerical model set-up

We use a finite element numerical model to solve for the steady-state 3D mantle velocity and temperature fields resulting from the surface divergence of three plates. The top surface of Model 1 is divided into the African, Antarctic, and Australian plates (Fig. 4). Fig. 1a shows clear lines of seafloor fabric discontinuities on the African and Antarctic plates, expanding in a V-shape away from the RTJ along the SWIR. These seafloor fabric discontinuities bound crust created at the SWIR during the eastward propagation of the RTJ. An analogous triple junction trace exists on the Australian Plate (Fig. 4b), but it is not as distinct as the traces on the African and Antarctic plates because of the similarity in spreading rate and near collinearity of the SEIR and CIR.

We fix the location of the triple junction in the center of Model 1, and prescribe the motions of the three plates with respect to the triple junction according to the RTJ velocity triangle calculated by [10]. The component of the plate motion vector perpendicular to each ridge is equal to the half-spreading rate and spreading direction of that ridge. For the top model surface, normal stress $\sigma_{zz} = 0$. For velocity boundary conditions on the vertical sides and the bottom of the model box, we prescribe the analytical solution for upwelling and horizontal velocity for each grid node as a function of depth and perpendicular distance from the appropriate ridge axis, using the 2D formulations of [39]. Temperature is assigned to be 0° and 1350°C on the top and bottom boundaries of the model, respectively, and the horizontal temperature gradients are set to zero on the vertical sides of the model domain.

The model box is 2000 km × 2000 km × 200 km (Fig. 4a), enabling us to investigate mantle flow and thermal fields along at least 1000 km of each ridge. The model box is discretized into 41 × 41 × 15 grid nodes, with highest horizontal resolution near the triple junction and greatest vertical resolution near the top surface of the box where velocity and temperature gradients are largest. In the horizontal direction, grid spacing ranges from 20 to 99 km, while vertical grid spacing increases from 5 to 29 km with depth.

To solve for mantle velocity and temperature, we use a 3D fluid dynamical code (ADINA, [40]) that solves the equation of continuity for an incompressible fluid:

$$\nabla \cdot \mathbf{v} = 0 \tag{1}$$

and the equation of momentum balance with constant viscosity and no buoyancy-driven flow:

$$\nabla P = \eta \nabla^2 \mathbf{v} + \rho \mathbf{g} \tag{2}$$

where $\mathbf{v}$ is velocity vector, P is fluid pressure, η is mantle viscosity, ρ is mantle density (3300 kg/m^3), and $\mathbf{g}$ is the acceleration of gravity. In these calculations, mantle viscosity is set to a constant 10^{21} Pa s. The steady-state temperature field is solved using:

$$\kappa \nabla^2 T + \mathbf{v} \nabla T = 0 \tag{3}$$

where velocity vector $\mathbf{v}$ is derived from the solution of Eq. 2, T is mantle temperature, and κ is thermal diffusivity (1 mm^2/s).

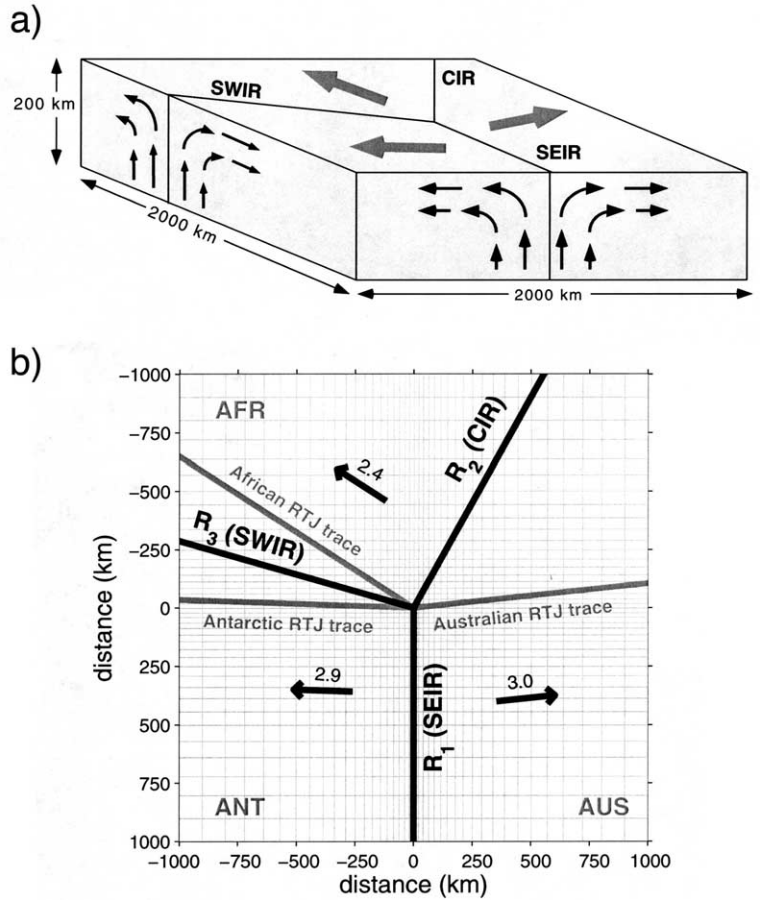

Fig. 4. (a) 3D schematic representation of the model domain. The positions of the SEIR, CIR, and SWIR are indicated with lines on the top of the model domain. The divergence of the Australian, Antarctic, and African plates about the RTJ is indicated by gray arrows. The model box is 2000×2000 km in the horizontal direction, and 200 km in depth. (b) The top surface of the set-up for Model 1. Flow within the model box is driven by the divergence of the African (AFR), Antarctic (ANT), and Australian (AUS) plates. The position of the triple junction is fixed in the model reference frame, and the motions of the three plates with respect to the triple junction are indicated by thick black arrows labeled with the divergence rate (cm/yr). The component of the plate motion vectors perpendicular to R_3 (SWIR), R_2 (CIR), or R_1 (SEIR) is equal to the half-spreading rate and local spreading direction of each ridge. RTJ traces represent accretionary boundaries dividing the crust created at two adjacent ridges. Light gray orthogonal lines represent every other numerical grid for the flow and temperature calculations.

4. Model results

4.1. Triple junction velocity and temperature fields

In Model 1, the divergence of three surface plates away from the triple junction is calculated to induce a component of flow along each of R_1, R_2, and R_3 (Fig. 5). This along-axis flow is strongest for the slowest-spreading ridge R_3 (SWIR), where it is directed away from the triple junction. At a representative location within the partial melting zone at 50 km depth and 300 km away from the triple junction, the magnitude of along-axis velocity is predicted to be 90% of upwelling velocity for R_3. A moderate component of along-axis velocity is present for R_2 (CIR) as well. At the corresponding location for R_2, along-axis velocity is 70% of upwelling velocity. In contrast, at the same location for R_1 (SEIR), the calculated

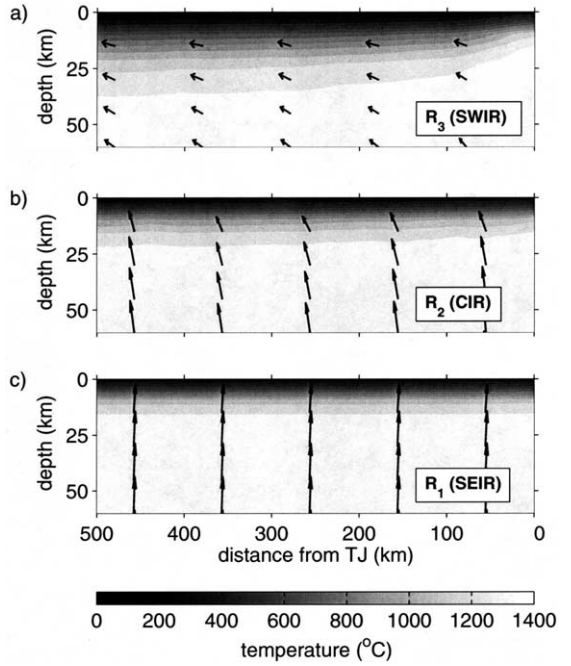

Fig. 5. Model-predicted mantle velocity, along the planes of the (a) R_3, (b) R_2, and (c) R_1 spreading branches. Note the strong component of along-axis velocity for R_3 (SWIR). In contrast, mantle motion is calculated to be almost completely dominated by vertical upwelling for R_1 (SEIR). Gray shading indicates calculated mantle temperature, with shading changes every 100°C.

mantle flow is nearly vertical, with along-axis velocity only 2% that of upwelling velocity.

The calculated upwelling velocity for the slowest-spreading R_3 increases significantly towards the triple junction (Fig. 6). At a far-field distance of 500 km from the triple junction, the calculated upwelling velocity for R_3 approximately equals that generated in the simpler case when two plates diverge with a half-rate of 0.7 cm/yr. However, within 200 km from the triple junction, upwelling velocity for R_3 increases more than threefold, approaching that of R_1. A similar, though less pronounced, increase in the upwelling velocity is also predicted for R_2.

Fig. 7a shows the calculated triple-junction temperature field at a depth of 32 km, within the zone of partial melting. The strong thermal signatures of the faster-spreading R_1 and R_2 are apparent. On the other hand, R_3 has lower overall axial temperatures, consistent with its ultra-slow spreading rate. However, beneath the axis of R_3, mantle temperature at 32-km depth is calculated to increase by 70–100°C towards the triple junction as a result of enhanced triple junction upwelling (Fig. 8a). In fact, for all depths, R_3 has the greatest temperature increase relative to the case of a single ridge (Fig. 9a).

In summary, far from the RTJ (>500 km), the calculated upwelling velocity and thermal fields of R_3 and R_2 are similar to the case of the simple divergence of two plates with corresponding half-spreading rates. However, both upwelling velocity and temperature for these two slower-spreading ridges are predicted to increase toward the triple junction to approach those of the fastest-spreading ridge. In contrast, upwelling velocity and temperature for R_1 are little affected by the presence of the other two ridges, maintaining magnitudes similar to the simpler single ridge case. Note that these model calculations predict little direct material transfer from the fastest-spreading ridge to the two slower-spreading ridges.

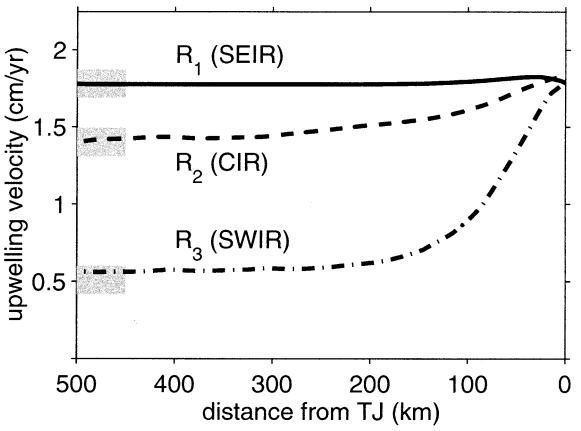

Fig. 6. The calculated upwelling velocity magnitude along R_1 (SEIR, solid line), R_2 (CIR, dashed line), and R_3 (SWIR, dash–dot line), at a depth of 75 km. For comparison, the magnitude of upwelling velocity driven by passive two-plate separation at the corresponding half-spreading rate is indicated by a light gray box on the left edge. Note that the magnitude of the upwelling velocity for R_3, and to a lesser extent R_2, increases toward the triple junction to approach R_1 upwelling velocity. Note also that R_1 upwelling velocity does not appear to be significantly changed by the presence of the other two ridges.

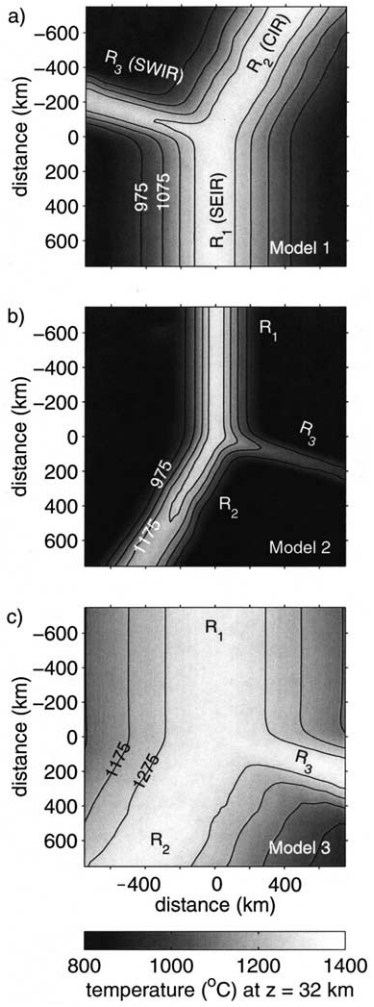

Fig. 7. Plan view of predicted temperature patterns for (a) Model 1 (RTJ), (b) Model 2 (similar to ATJ), and (c) Model 3 (similar to GTJ) at a depth of 32 km. Note that for all three triple junctions, the two fastest-spreading ridges dominate the thermal structure of the region, while the temperature of the slowest-spreading ridge increases toward the triple junction.

4.2. *Effects of absolute magnitude of spreading rates*

To determine the effects of changing the absolute magnitude of the spreading rates for the three ridges while keeping their relative ratios unchanged, we calculate velocity field and temperature for the same model geometry described in Section 3, but scale the surface divergence velocities by a factor of either $1/c_o$ (Model 2) or c_o (Model 3), where $c_o = 2.4$. Application of these scaling factors roughly yields the spreading rates for the ridges of the ATJ and GTJ, respectively. Therefore, in considering the models in a geographical context, it may be useful to refer to R_1, R_2, and R_3 as N. MAR, S. MAR, and Ter. R., respectively, in Model 2 (ATJ) and as N. EPR, S. EPR, and GSC, respectively, in Model 3 (GTJ). However, it should be made clear that the comparison of model geometry to the actual ATJ and GTJ configurations is not rigorous, because the observed ridge angles are slightly differ-

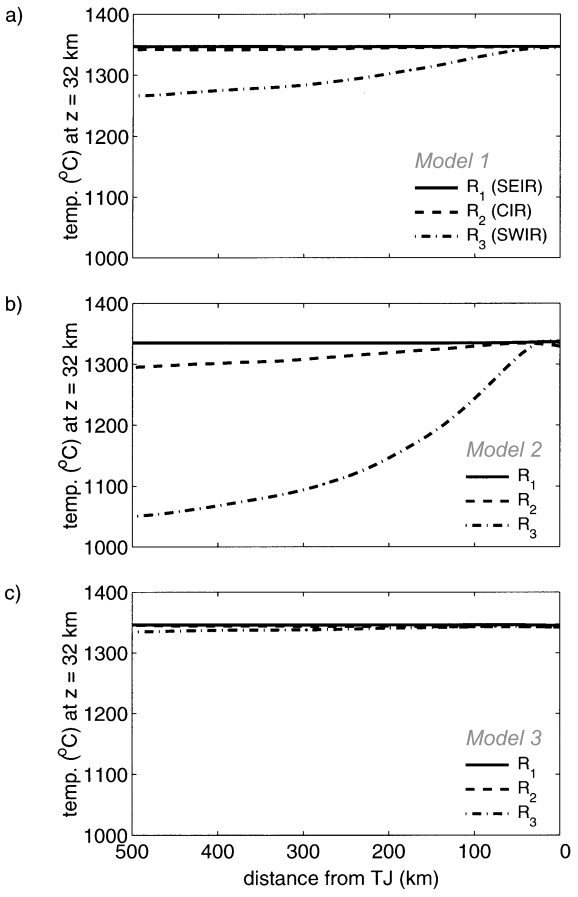

Fig. 8. Along-axis profiles of temperature at a depth of 32 km for (a) Model 1 (RTJ), (b) Model 2 (similar to ATJ), and (c) Model 3 (similar to GTJ). Note that in all three panels, the predicted temperature increase toward the triple junction is most pronounced for the slowest-spreading branch (dash–dot line).

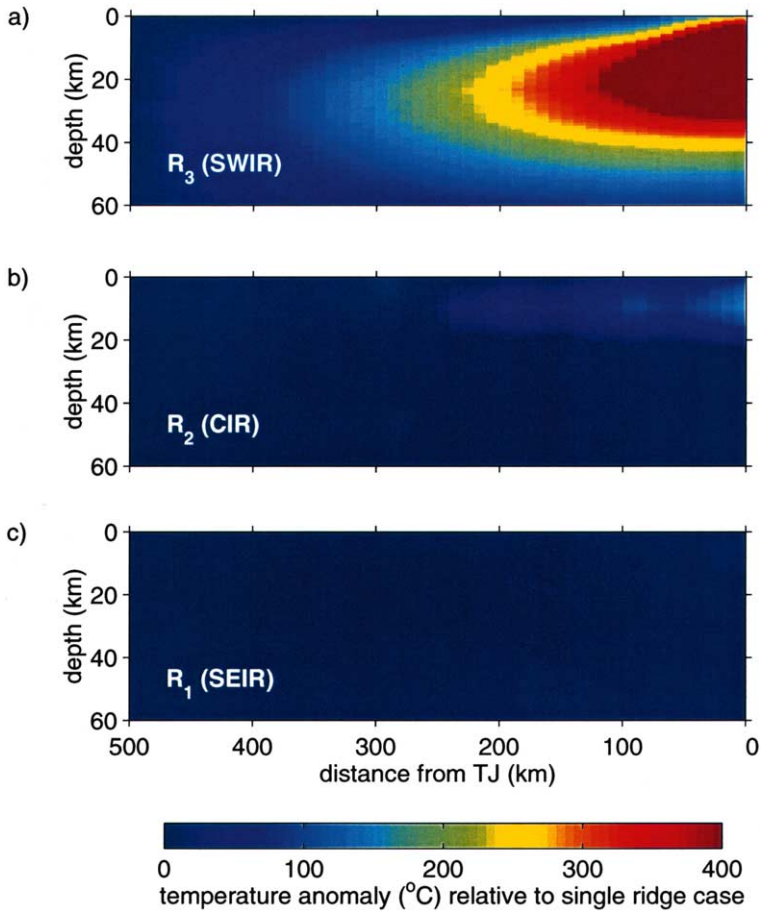

Fig. 9. The calculated temperature anomaly caused by triple junction flow for (a) R_3 (SWIR), (b) R_2 (CIR), and (c) R_1 (SEIR). Temperature anomaly was determined by subtracting the temperature–depth section calculated for a single ridge case with the spreading rate of R_1, R_2, or R_3 from the temperature–depth section calculated for the ridges as shown in Fig. 5. Note that the slowest-spreading ridge R_3 has the most pronounced thermal anomaly with respect to the single ridge case, while the predicted thermal anomaly for R_2 is small and confined to the immediate vicinity of the triple junction. In contrast, the thermal anomaly for R_1 is negligible.

ent than in the models, and therefore only qualitative inferences about the ATJ and GTJ should be drawn from the model predictions.

The results of the thermal calculations for Models 2 and 3 are shown in Figs. 7b-c and 8b-c. Because the overall spreading rates are slower in Model 2 than in Model 1, the calculated temperatures are correspondingly lower in Model 2 at a given depth (Fig. 7). However, the predicted temperature increase along the ultra-slow spreading R_3 in Model 2 is dramatic. Within 500 km of the triple junction, temperature within the partial melting region is calculated to increase by more than 250°C, approaching the value for R_1 (Fig. 8b). Axial temperature is also predicted to increase for R_2, although the magnitude of the increase is considerably less than that of R_3 because of the similarity in spreading rate between R_1 and R_2. Before these model results are applied to the ATJ, however, it is important to mention that the presence of the Azores plume is expected to substantially alter these thermal patterns. The present location of the Azores plume is thought to be in the vicinity of Faial Island, to the east of the

triple junction and south of the Ter. R. [22–23]. Because of the 3D nature of mantle flow around the triple junction, a plume situated slightly south of R_3 in Model 2 is expected to cause more plume influence on the S. MAR than the N. MAR. Such north–south asymmetry is consistent with geologic observations (e.g., [24,26–28]).

Model 3 (Fig. 7c) represents two fast-spreading ridge branches intersected by an intermediate-spreading ridge, similar to the case of the GTJ. Since all three ridges spread at relatively rapid rates, the thermal contrast between them is not as pronounced as for Model 1 or Model 2. Correspondingly, no significant along-axis temperature increase is predicted for R_3 (Fig. 8c). Instead, at depths within the partial melting zone (30–80 km), all three ridges maintain temperatures close to their temperature far away from the triple junction. Thus this model predicts that the thermal state near the GTJ is not altered significantly by the presence of the triple junction.

4.3. RTJ thermal topography

We next compare the predictions from Model 1 to the observed bathymetric trends of the ridges near the RTJ. East of the Melville Fracture Zone at 61°E, the SWIR achieves its greatest axial depth (Fig. 10a). Cannat et al. [41] suggest that this extreme depth can be explained by mantle temperatures that are significantly cooler than normal, with a concomitant decrease in magmatic production. In the immediate vicinity of the RTJ, however, the maximum depth of the SWIR axis shallows significantly (Fig. 10b). To determine if our model predictions are consistent with the observed shallowing, we calculate model topography resulting from mantle density variations due to thermal structure, and compare the calculated axial profiles to satellite-gravity predicted bathymetry [42]. We employ predicted bathymetry in the comparison because, although the SWIR and CIR have continuous or nearly continuous axial ship-track coverage over the region shown in Fig. 10a, similar coverage for the SEIR is not available.

It is difficult to precisely determine the relative importance of the various factors that contribute to axial bathymetry (e.g., mantle thermal variations, crustal thickness variations, and dynamically supported topography) because at present there are no seismic data around the RTJ to constrain crustal thickness. We recognize that while this modeling is designed to explore long-wavelength axial trends, local tectonics exert an important control on lithospheric processes near the RTJ. We note, for example, that detailed geological studies of the SWIR near the RTJ [38,43] suggest the existence of a propagator feature that terminates ~50–100 km west of the triple junction, with a rift tip that is locally depressed and supported by dynamic stresses [44]. Between this anomalously deep rift tip and the triple junction, seafloor depth recovers to more average values. Likewise, large rift-flank uplifts suggest the importance of flexural and dynamic stresses.

Despite the uncertainty inherent in decomposing SWIR axial topography, mantle Bouguer anomaly (MBA) can be used to aid the evaluation of the relative contributions of dynamic and isostatic topography to ridge-axis bathymetry. MBA reflects density variations resulting from changes in crustal thickness and/or mantle temperature [45,46]. Fig. 11 shows MBA around the RTJ, extracted from a map published in Georgen et al. [35], as well axial profiles of MBA for the SWIR and SEIR. Although short-wavelength variations are present, to first order the SWIR MBA profile becomes more negative toward the triple junction, while MBA along the SEIR remains relatively constant and more negative than that of the SWIR. The decrease in MBA along the SWIR toward the RTJ is consistent with increasing mantle temperature and/or crustal thickness toward the triple junction, suggesting that the axial topography is not purely dynamically supported. Gravity studies along the GSC in the vicinity of the Galapagos plume [18] and along the Reykjanes Ridge near Iceland [47] suggest that mantle thermal variations contribute approximately 25–30% to the topography and mantle Bouguer gravity signal, with the rest attributable to crustal thickness variations. Accordingly, we calculate an isostatic topography profile, assuming that thermal variations account for 30% of the overall ridge topography.

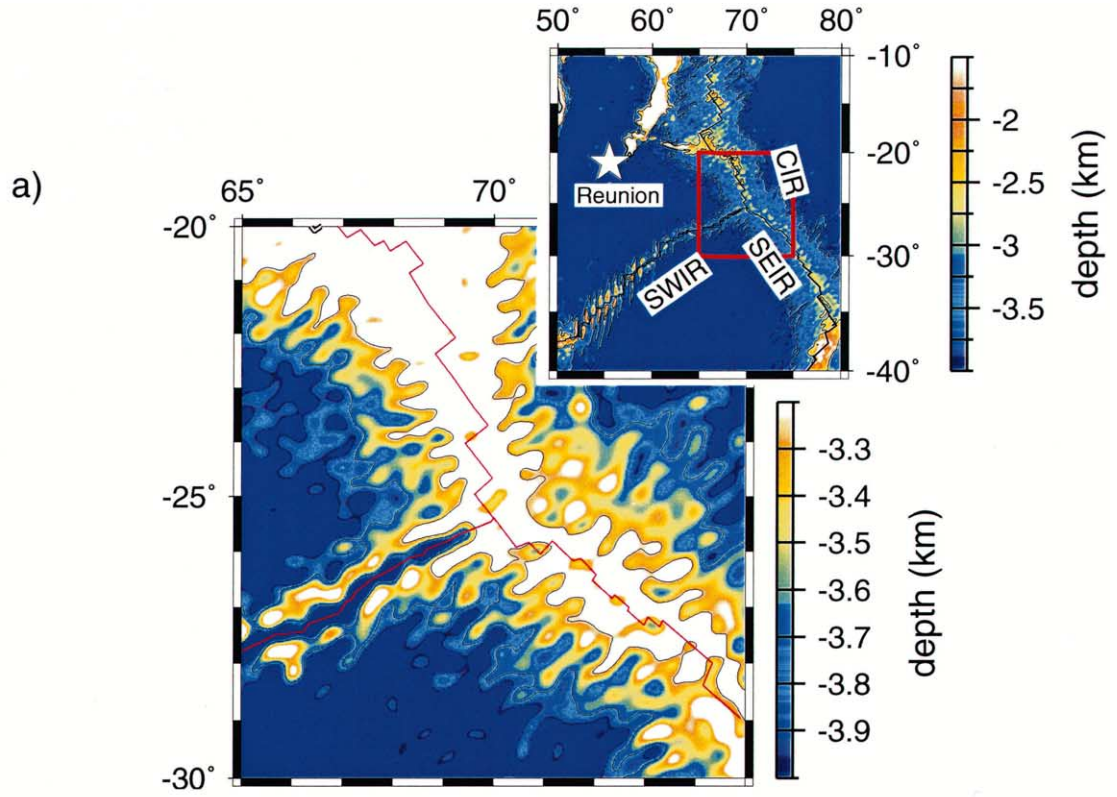
a)
50°
60°
70°
80°
-10°
-20°
-30°
-40°
Reunion
CIR
SEIR
SWIR
-2
-2.5
-3
-3.5
depth (km)
65°
70°
-20°
-25°
-30°
-3.3
-3.4
-3.5
-3.6
-3.7
-3.8
-3.9
depth (km)

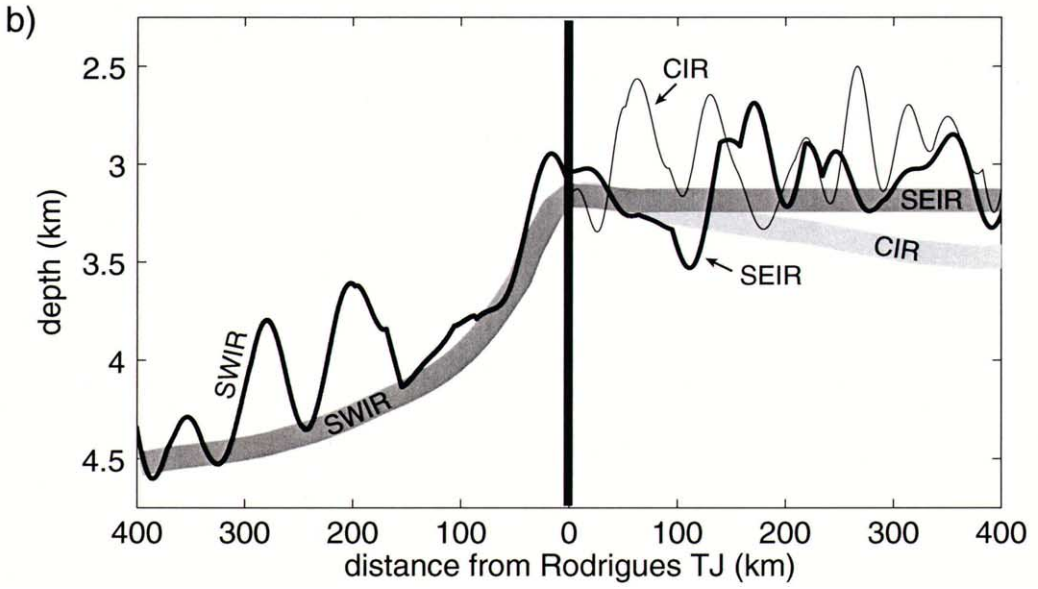
b)
2.5
3
3.5
4
4.5
depth (km)
CIR
SEIR
CIR
SEIR
SWIR
SWIR
400
300
200
100
0
100
200
300
400
distance from Rodrigues TJ (km)

The topographic variation Δh can be calculated as:

$$\Delta h = \int \alpha \rho_m (T - T_o)/(\rho_c - \rho_w) dz \quad (4)$$

where the coefficient of thermal expansion $\alpha = 3 \times 10^{-5}$°C^{-1}, reference mantle density ρ_m = 3300 kg/m^3, reference crustal density ρ_c = 2700 kg/m^3, water density ρ_w = 1030 kg/m^3, T is mantle temperature, and reference mantle temperature T_o = 1350°C at depth z = 200 km. We assume that vertical columns of mantle are in isostatic equilibrium at depth z = 200 km.

Fig. 10b suggests that the general long-wavelength shallowing of the SWIR axis toward the RTJ is consistent with the isostatic topography predicted by the triple junction thermal model. Similarly, despite fluctuations about a mean depth of approximately 3.2 km, SEIR axial depth neither increases nor decreases systematically away from the RTJ. Again, model-predicted thermal topography is consistent with this observation (Fig. 10b). Meanwhile, whereas CIR axial depth is observed to be relatively constant, or perhaps even shallowing, away from the RTJ, model results predict a deepening trend. We attribute this discrepancy to the influence of the off-axis Reunion hotspot on the CIR. The Reunion hotspot is associated with anomalously shallow CIR topography along an axial section centered at ~20°S [48].

Further test of the predicted temperature structure near a triple junction could come from regional geochemical studies. For example, Model 1 predicts progressively greater extents of melting along the SWIR towards the RTJ. Such variations could be detected from $Na_{8.0}$ and other geochemical systematics (e.g., [49,50]). This model also suggests that $Na_{8.0}$ should be higher for the SWIR than the SEIR or CIR far away from the RTJ. Currently, however, there are few published studies on major element data trends along the SWIR in the immediate vicinity of the RTJ. However, a study of SWIR peridotites between 52°E and 69°E [51] suggests that the maximum extent of mantle melting increases moderately from 62°E to 69°E, consistent with model predictions.

5. Discussion

The primary goal of this investigation is to quantify the long-wavelength patterns of passive mantle upwelling and temperature beneath an RRR triple junction and to contrast them with the patterns of a single ridge. We purposefully selected to focus on purely passive upwelling because this approach isolates the simplest physics inherent to the triple junction problem. Similar to the progressive approach used in developing single ridge models (e.g., [5–7,52–53]), subsequent triple junction models may investigate the additional effects of variable viscosity, thermal buoyancy, melt retention/depletion buoyancy, melting, and the like. These subsequent studies can specifically explore how the inclusion of these additional factors alters the essential triple junction features predicted in this study, such as strong along-axis flow and increased upwelling rate and temperature along the slowest-spreading ridge. In the

←

Fig. 10. (a) Filtered bathymetry of the RTJ. Filtered bathymetry was calculated by applying a 2D lowpass filter with a cutoff wavelength of 50 km to the map displayed in the inset. Contours delineate 3.25 and 3.75 km depth. Inset: Bathymetry map for the RTJ region. Predicted bathymetry data were extracted from the Smith and Sandwell [42] database, and contours delineate 2.75 and 3.75 km depth. (b) Along-axis profiles of filtered bathymetry along the SWIR, SEIR, and CIR. To the right of the vertical black bar, which marks the triple junction, the SEIR axial profile is shown with a thick black line, while the CIR profile is indicated with a thin black line. Dark (SWIR and SEIR) and light (CIR) thick gray curves indicate model-predicted isostatic topography due to mantle thermal variations. Calculation of isostatic topography is described in the text. Note that the SWIR ridge axis shallows significantly within a distance of ~150 km from the RTJ, a general trend which is mirrored by the model predictions. Similarly, despite fluctuations at about a mean depth of ~3.2 km, the SEIR axis does not systematically shallow or deepen. This trend is also reflected in the flatness of the predicted isostatic topography. Discrepancy between the model-predicted isostatic topography and observed axial depth for the CIR may be attributed to the Reunion hotspot, which was not considered in the present models.

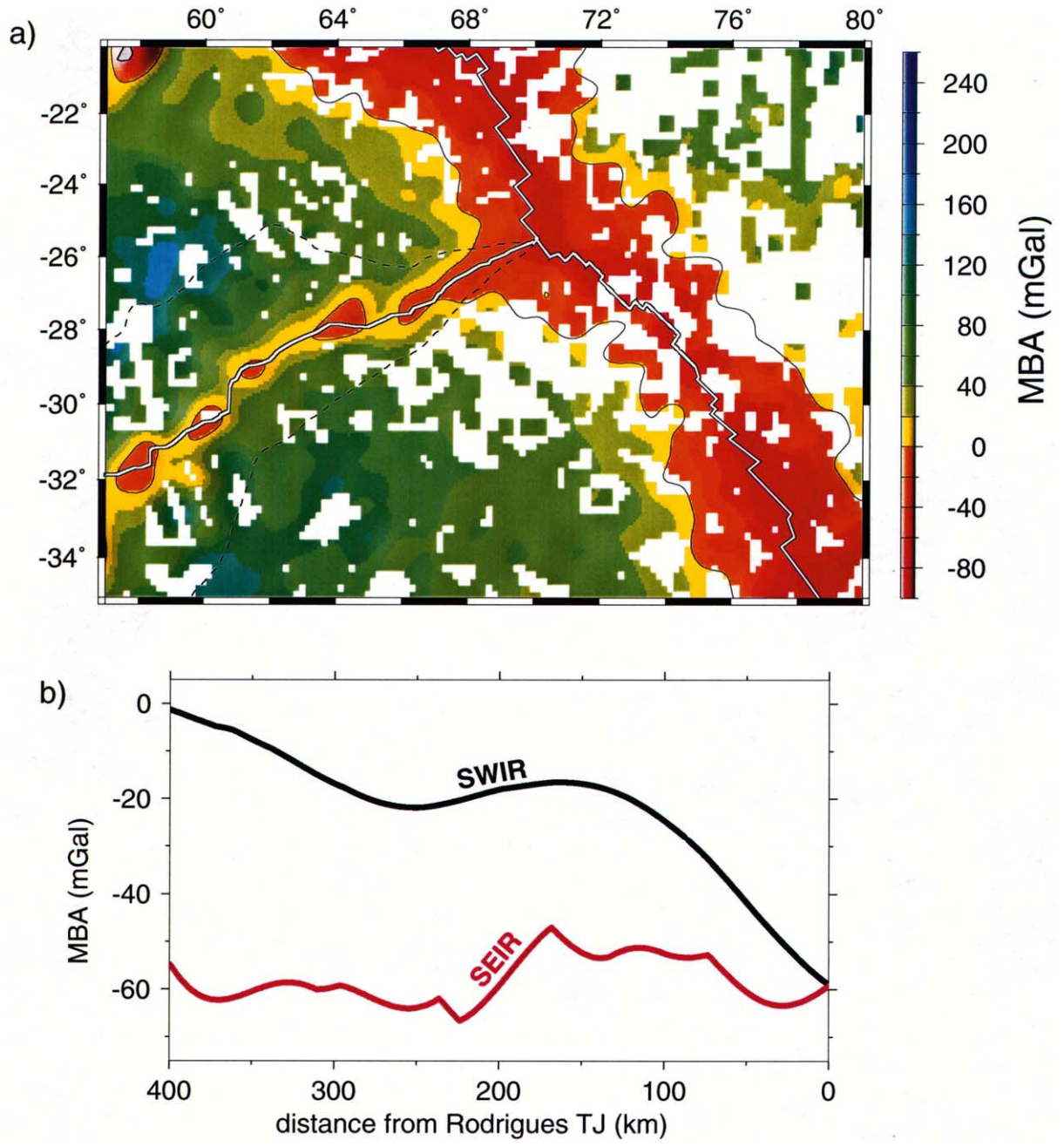

Fig. 11. (a) Filtered MBA in the vicinity of the RTJ. MBA map was extracted from Ref. [35]; details of the MBA calculation can be found therein. Filtered MBA was calculated by applying to the unfiltered map a 2D lowpass filter with cutoff wavelength 100 km. Grid nodes without shiptrack control within a 10′ radius are masked with white. Dashed lines indicate triple junction traces. (b) Along-axis profiles of filtered MBA for the SWIR (black) and SEIR (red). Note that MBA generally decreases toward the triple junction along the SWIR, whereas MBA values of the SEIR are relatively constant and more negative than those of the SWIR. The MBA profile along the CIR was not plotted because of the complicating effects of the Reunion hotspot on the CIR away from the RTJ. Nevertheless, the MBA map in panel a shows that the MBA values along the CIR are, overall, also more negative than those of the SWIR.

following paragraphs we qualitatively discuss the potential effects of a few factors not incorporated in the present models.

Melting and crustal thickness variations: Testing these models of mantle flow and temperature structure beneath a triple junction can be facilitated by calculation of the associated melting patterns and magmatic crustal thickness. Previous studies have calculated crustal thickness beneath a single ridge by first computing the distribution of partial melt beneath the ridge axis and then integrating all melt generated in a plane perpendicular to the spreading axis (e.g., [5,18]). Similar calculations for a triple junction are likely to be complicated and should consider additional factors, such as the partitioning of melt between the three spreading branches and the melting history of mantle rocks in a highly 3D flow geometry.

Variable viscosity and buoyancy: Previous models of a single ridge (e.g., [6]) have illustrated that if mantle viscosity is pressure- and temperature-dependent, the predicted mantle upwelling is both stronger and more localized to the region immediately below the ridge axis than in the case of constant mantle viscosity. The predicted across-axis width of the axial high upwelling velocity zone for temperature- and pressure-dependent viscosity is approximately 20–30% narrower than that for the constant viscosity case [6]. By analogy, we expect that if pressure- and temperature-dependent viscosity is introduced in the model, the zone of increased upwelling and temperature along R_3 is likely to be 20–30% narrower than the current model of constant viscosity.

Similarly, single-ridge models have illustrated that buoyancy forces due to thermal, melt retention, and melt depletion effects can increase the overall upwelling velocity and narrow the upwelling zone [52,54]. Thus it is possible that the introduction of buoyancy forces may also decrease the length of triple junction influence along R_3. Both the variable viscosity and buoyancy effects should enhance the overall upwelling velocity in the immediate proximity of the triple junction. Such enhanced upwelling, however, may be counteracted by the effects of diffuse spreading and ridge reorganizations described next.

'Virtual' vs. actual triple point: Several high-resolution studies of RRR triple junctions have shown that, rather than meeting at a strict geometrical point, the three spreading branches often fail to connect. Evidence for such ridge non-connectivity is found at the BTJ [29], ATJ [2], and RTJ [37,38], among others. Commonly, the slowest-spreading branch is separated from a triple junction by a zone of diffuse deformation, leading to the suggestion that, at a local scale (<100 km away from the triple point), spreading at an RRR triple junction may occur throughout a broad area, rather than linearly along three well-defined ridges. Observations further suggest that the width of the diffuse spreading zone may vary with time. It is envisioned that periods when the triple junction migrates away from the end of the slowest-spreading ridge may alternate with periods when the slowest ridge propagates rapidly to be connected to the faster ridges [3,37]. The failure of the slowest-spreading ridge to be connected to the faster ridges at all times is expected to reduce the overall upwelling beneath the triple junction, and thus counteract the enhanced upwelling caused by variable viscosity and buoyancy effects.

Quantitative estimation of the relative importance of variable viscosity and buoyancy (in increasing crustal production) versus lithospheric effects (in decreasing crustal production) is difficult without additional modeling. However, in light of a lack of seismic crustal thickness estimates along the SWIR near the RTJ, off-axis gravity can be used to explore the history of crustal accretion [55]. More specifically, enhanced crustal production could result in variations of MBA across the African and Antarctic triple junction traces, with relatively more negative MBA on the side of the trace created by the SWIR. However, such systematic variation of MBA across the triple junction traces is not readily apparent (Fig. 11), suggesting that the structure of the triple junction traces might be controlled by complex interplay between various mantle and lithospheric processes that are still poorly understood.

Detailed ridge segment geometry: The models described in this investigation purposefully make use of a simplified ridge geometry to isolate the

long-wavelength mantle dynamics arising from the conjunction of three divergent plates. More detailed ridge geometry incorporating segmentation at wavelengths less than ~100 km will add local complexity to the 3D flow fields. However, we anticipate these effects to be limited only to ridge segment scales.

6. Conclusions

The results of this investigation yield the following main conclusions regarding mantle flow and temperature structure beneath and RRR triple junction:

(1) When the slowest-spreading ridge intersects two near-collinear faster-spreading ridges quasi-orthogonally, such as at the Rodrigues, Azores, and Galapagos triple junctions, the upwelling velocity and temperature along the slowest-spreading branch are calculated to increase toward the triple junction, approaching the greater upwelling rate and higher temperature of the fastest-spreading branch. In contrast, the velocity and thermal fields for the fastest-spreading ridge are not significantly different from the case of a single ridge with a corresponding spreading rate.

(2) For a model geometry resembling the RTJ, upwelling velocity along the slowest-spreading SWIR is predicted to increase more than threefold within 200 km of the triple junction. A strong component of along-axis flow, directed away from the triple junction, is also predicted. Similarly, model calculations suggest temperature increases by ~75°C along the SWIR axis at depths within the partial melting zone. Isostatic models based on the predicted temperature fields can qualitatively explain the long-wavelength shallowing of the SWIR axis towards the triple junction and the relatively shallow depths of the SEIR and CIR axes.

(3) For ridge branches with the same geometry as the RTJ, but with a factor of 2.4 faster spreading rate for each of the ridge branches (a configuration similar to the GTJ), the predicted velocity and temperature differences between the three ridges are less pronounced. However, when spreading rates are a factor of 2.4 slower (a configuration similar to the ATJ), the predicted differences between the slowest- and fastest-spreading ridges are increased. Therefore, the geodynamical effects of triple junction geometry are likely more important for the ATJ than the GTJ.

Acknowledgements

We wish to thank the members of the Geodynamics and Tectonics Group at WHOI for many useful suggestions and insightful comments. We also thank Henry Dick for many interesting conversations about triple junctions, and Bob Detrick and Maria Zuber for helpful suggestions. Constructive reviews by Roger Searle and Fernando Martinez improved the manuscript. This work was supported by NSF grants OCE-9811924 and OCE-9907630. Woods Hole Oceanographic Institution contribution number 10635.*[AC]*

References

[1] N.C. Mitchell, L.M. Parson, The tectonic evolution of the Indian Ocean triple junction, Anomaly 6 to present, J. Geophys. Res. 98 (1993) 1793–1812.
[2] R.C. Searle, Tectonic pattern of the Azores spreading center and triple junction, Earth Planet. Sci. Lett. 51 (1980) 415–434.
[3] R.C. Searle, J. Francheteau, Morphology and tectonics of the Galapagos triple junction, Mar. Geophys. Res. 8 (1986) 95–129.
[4] J.G. Sclater, C. Bowin, R. Hey, H. Hoskins, J. Peirce, J. Phillips, C. Tapscott, The Bouvet Triple Junction, J. Geophys. Res. 81 (1976) 1857–1869.
[5] J. Phipps Morgan, D.W. Forsyth, 3-D flow and temperature perturbations due to transform offset: effects on oceanic crustal and upper mantle structure, J. Geophys. Res. 93 (1988) 2955–2966.
[6] Y. Shen, D.W. Forsyth, The effects of temperature- and pressure-dependent viscosity on three-dimensional passive flow of the mantle beneath a ridge-transform system, J. Geophys. Res. 97 (1992) 19727–19728.
[7] D.W. Sparks, E.M. Parmentier, The structure of three-dimensional convection beneath oceanic spreading centers, Geophys. J. Int. 112 (1993) 81–91.
[8] M. Rabinowicz, S. Rouzo, J.C. Sempere, C. Rosemberg, Three-dimensional mantle flow beneath mid-ocean ridges, J. Geophys. Res. 98 (1993) 7851–7869.
[9] D.P. McKenzie, W.J. Morgan, Evolution of triple junctions, Nature 224 (1969) 125–133.

[10] C. Tapscott, P. Patriat, R.L. Fisher, J.G. Sclater, H. Hoskins, B. Parsons, The Indian Ocean Triple Junction, Geophys. Res. 85 (1980) 3969–4723.
[11] P. Patriat, L. Parson, A survey of the Indian Ocean Triple Junction trace within the Antarctic Plate: implications for the junction evolution since 15 Ma, Mar. Geophys. Res. 11 (1989) 89–100.
[12] J.G. Sclater, R.L. Fisher, Ph. Patriat, C. Tapscott, B. Parsons, Eocene to recent development of the Southwest Indian Ridge, a consequence of the evolution of the Indian Ocean triple junction, Geophys. J. R. Astron. Soc. 64 (1981) 587–604.
[13] P. Patriat, D. Sauter, M. Munschy, L. Parson, A survey of the Southwest Indian Ridge axis between Atlantis II Fracture Zone and the Indian Ocean Triple Junction: regional setting and large scale segmentation, Mar. Geophys. Res. 19 (1997) 457–480.
[14] R.N. Hey, G.L. Johnson, A. Lowrie, Recent plate motions in the Galapagos area, Geol. Soc. Am. Bull. 88 (1977) 1385–1403.
[15] P. Lonsdale, Structural pattern of the Galapagos Microplate and evolution of the Galapagos triple junctions, J. Geophys. Res. 93 (1988) 13551–13574.
[16] J.-G. Schilling, R.H. Kingsley, J.D. Devine, Galapagos hot spot-spreading center system. 1. Spatial petrological and geochemical variations (83°W–101°E), J. Geophys. Res. 87 (1982) 5593–5610.
[17] S.P. Verma, J.-G. Schilling, D.G. Waggoner, Neodymium isotopic evidence for Galapagos hotspot-spreading centre system evolution, Nature 306 (1983) 654–657.
[18] G. Ito, J. Lin, Mantle temperature anomalies along the present and paleoaxes of the Galapagos spreading center as inferred from gravity analysis, J. Geophys. Res. 100 (1995) 3733–3745.
[19] J.P. Canales, J.J. Danobeitia, R.S. Detrick, E.E.E. Hooft, R. Bartolome, D.F. Naar, Variations in axial morphology along the Galapagos spreading center and the influence of the Galapagos hotspot, J. Geophys. Res. 102 (1997) 27341–27354.
[20] J.P. Canales, G. Ito, R.S. Detrick, J. Sinton, T. Blacic, M. Behn, J. Lin, Origin of the Galapagos swell: bathymetry, gravity, and seismic constraints along the Galapagos Spreading Center, EOS, Trans. AGU 81 (2000) F1095.
[21] D.C. Krause, N.D. Watkins, North Atlantic crustal genesis in the vicinity of the Azores, Geophys. J. R. Astron. Soc. 19 (1970) 261–283.
[22] Y. Zhang, T. Tanimoto, Ridges, hotspots, and their interactions as observed in seismic velocity maps, Nature 355 (1992) 45–49.
[23] J.-G. Schilling, Fluxes and excess temperatures of mantle plumes inferred from their interaction with migrating mid-ocean ridges, Nature 352 (1991) 397–403.
[24] L. Dosso, H. Bougault, J.-L. Joron, Geochemical morphology of the North Mid-Atlantic Ridge, 10 degrees–24 degrees N: trace element–isotope complementarity, Earth Planet. Sci. Lett. 120 (1993) 443–462.
[25] G. Ito, J. Lin, Oceanic spreading center-hotspot interactions: constraints from along-isochron bathymetric and gravity anomalies, Geology 23 (1995) 657–660.
[26] R.S. Detrick, H.D. Needham, V. Renard, Gravity anomalies and crustal thickness variations along the Mid-Atlantic Ridge between 33°N and 40°N, J. Geophys. Res. 100 (1995) 3767–3787.
[27] J. Goslin, Triatnord Scientific Party, Extent of Azores plume influence on the Mid-Atlantic Ridge north of the hotspot, Geology 27 (1999) 991–994.
[28] M. Cannat, A. Briais, C. Deplus, J. Escartin, J. Georgen, J. Lin, S. Mercouriev, C. Meyzen, M. Muller, G. Pouliquen, A. Rabain, P. daSilva, Mid-Atlantic Ridge-Azores hotspot interactions: along-axis migration of a hotspot-derived event of enhanced magmatism 10 to 4 Ma ago, Earth Planet. Sci. Lett. 173 (1999) 257–269.
[29] M. Ligi, E. Bonatti, G. Bortoluzzi, G. Carrara, P. Fabretti, D. Penitenti, D. Gilod, A.A. Peyve, S. Skolotnev, N. Turko, Death and transfiguration of a triple junction in the south Atlantic, Science 276 (1997) 243–245.
[30] C.J.H. Hartnady, A.P. leRoex, Southern ocean hotspot tracks and the Cenozoic absolute motion of the African, Antarctic, and South American plates, Earth Planet. Sci. Lett. 75 (1985) 245–257.
[31] J. Douglass, J.G. Schilling, R.H. Kingsley, C. Small, Influence of the Discovery and Shona mantle plumes on the southern Mid-Atlantic Ridge: rare Earth evidence, Geophys. Res. Lett. 22 (1995) 2893–2986.
[32] C. Small, Observations of ridge-hotspot interactions in the Southern Ocean, J. Geophys. Res. 100 (1995) 17931–17946.
[33] M. Moreira, T. Staudacher, P. Sarda, J.G. Schilling, C.J. Allegre, A primitive plume neon component in MORB: the Shona Ridge anomaly, South Atlantic (51–52 S), Earth Planet. Sci. Lett. 133 (1995) 367–377.
[34] N.C. Mitchell, R.A. Livermore, Spiess Ridge: an axial high on the slow spreading Southwest Indian Ridge, J. Geophys. Res. 103 (1998) 15457–15471.
[35] J. Georgen, J. Lin, H.J.B. Dick, Evidence from gravity anomalies for interactions of the Marion and Bouvet hotspots with the Southwest Indian Ridge: effects of transform offsets, Earth Planet. Sci. Lett. 187 (2001) 283–300.
[36] N.H. Sleep, Hotspots and mantle plumes: some phenomenology, J. Geophys. Res. 95 (1990) 6715–6736.
[37] V. Mendel, D. Sauter, Ph. Patriat, M. Munschy, Relationship of the Central Indian Ridge segmentation with the evolution of the Rodrigues Triple Junction for the past 8 Myr, J. Geophys. Res. 105 (2000) 16563–16575.
[38] N.C. Mitchell, Distributed extension at the Indian Ocean triple junction, J. Geophys. Res. 96 (1991) 8019–8043.
[39] I. Reid, H.R. Jackson, Oceanic spreading rate and crustal thickness, Mar. Geophys. Res. 5 (1981) 165–171.
[40] K.-J. Bathe, Finite Element Procedures, Prentice Hall, Upper Saddle River, NJ, 1996, 1037 pp.
[41] M. Cannat, C. Rommevaux-Jestin, D. Sauter, C. Deplus, V. Mendel, Formation of the axial relief at the very slow spreading Southwest Indian Ridge (49 degrees to 69 degrees E), J. Geophys. Res. 104 (1999) 22825–22843.

[42] W.H.F. Smith, D. Sandwell, Global sea floor topography from satellite altimetry and ship depth soundings, Science 277 (1997) 1956–1962.
[43] B.P. West, H. Fujimoto, C. Honsho, K. Tamaki, J.C. Sempere, A three-dimensional gravity study of the Rodrigues triple junction and Southeast Indian Ridge, Earth Planet. Sci. Lett. 133 (1995) 175–184.
[44] J. Phipps Morgan, E.M. Parmentier, Causes and rate-limiting mechanisms of ridge propagation: a fracture mechanics model, J. Geophys. Res. 90 (1985) 8603–8612.
[45] B.Y. Kuo, D.W. Forsyth, Gravity anomalies of the ridge-transform system in the South Atlantic between 31 and 34.5°: upwelling centers and variations in crustal thickness, Mar. Geophys. Res. 10 (1988) 205–232.
[46] J. Lin, G.M. Purdy, H. Schouten, J.-C. Sempere, C. Zervas, Evidence from gravity data for focused magmatic accretion along the Mid-Atlantic Ridge, Nature 344 (1990) 627–632.
[47] G. Ito, J. Lin, C.W. Gable, Dynamics of mantle flow and melting at a ridge-centered hotspot: Iceland and the Mid-Atlantic Ridge, Earth Planet. Sci. Lett. 144 (1996) 53–74.
[48] A. Briais, Structural analysis of the segmentation of the Central Indian Ridge between 20°30′S and 25°30′S (Rodriguez Triple Junction), Mar. Geophys. Res. 17 (1995) 431–467.
[49] H.J.B. Dick, R.L. Fisher, W.B. Bryan, Mineralogic variability of the uppermost mantle along mid-ocean ridges, Earth Planet. Sci. Lett. 69 (1984) 88–106.
[50] E.M. Klein, C.H. Langmuir, Global correlations of ocean ridge basalt chemistry with axial depth and crustal thickness, J. Geophys. Res. 92 (1987) 8089–8115.
[51] M. Seyler, M. Cannat, The composition of dredged peridotites and the extent of mantle melting beneath the eastern portion of the Southwest Indian Ridge (52 to 69 E), EOS Trans. AGU 79 (1998) F878.
[52] K. Barnouin-Jha, E.M. Parmentier, D.W. Sparks, Buoyant mantle upwelling and crustal production at oceanic spreading centers: on-axis segmentation and off-axis melting, J. Geophys. Res. 102 (1997) 11979–11989.
[53] M.G. Braun, G. Hirth, E.M. Parmentier, The effects of deep damp melting on mantle flow and melt generation beneath mid-ocean ridges, Earth Planet. Sci. Lett. 176 (2000) 339–356.
[54] W. Su, W.R. Buck, Buoyancy effects on mantle flow under mid-ocean ridges, J. Geophys. Res. 98 (1993) 12191–12205.
[55] R.A. Pockalny, R.L. Larson, R.F. Viso, L.J. Abrams, Bathymetry and gravity data across a mid-Cretaceous triple junction trace in the southwest Pacific basin, Geophys. Res. Lett. 29 (2002) 10.1029/2001GL013517.
[56] R.D. Mueller, W.R. Roest, J.-Y. Royer, L.M. Gahagan, J.G. Sclater, Digital isochrons of the world's ocean floor, J. Geophys. Res. 102 (1997) 3211–3214.
[57] D.T. Sandwell, W.H.F. Smith, Marine gravity anomaly from Geosat and ERS 1 satellite altimetry, J. Geophys. Res. 102 (1997) 10039–10054.